Available online at www.sciencedirect.com

ScienceDirect

Journal of Materiomics 1 (2015) 124–133

www.ceramsoc.com/en/

www.journals.elsevier.com/journal-of-materiomics/

Dual Z-scheme charge transfer in TiO_2–Ag–Cu_2O composite for enhanced photocatalytic hydrogen generation

Junwei Fu [a], Shaowen Cao [a,*], Jiaguo Yu [a,b,*]

[a] State Key Laboratory of Advanced Technology for Materials Synthesis and Processing, Wuhan University of Technology, Wuhan, 430070, China
[b] Department of Physics, Faculty of Science, King Abdulaziz University, Jeddah, 21589, Saudi Arabia

Received 1 January 2015; revised 6 January 2015; accepted 20 February 2015
Available online 24 April 2015

Abstract

Photocatalytic hydrogen generation is one of the most promising solutions to convert solar power into green chemical energy. In this work, a multi-component TiO_2–Ag–Cu_2O composite was obtained through simple impregnation-calcination of Cu_2O and subsequent photodeposition of Ag onto electrospun TiO_2 nanotubes. The resulting TiO_2–Ag–Cu_2O photocatalyst exhibits excellent photocatalytic H_2 evolution activity due to the synergetic effect of Ag and Cu_2O on electrospun TiO_2 nanotubes. A dual Z-scheme charge transfer pathway for photocatalytic reactions over TiO_2–Ag–Cu_2O composite was proposed and discussed. This work provides a prototype for designing Z-scheme photocatalyst with Ag as an electron mediator.

Keywords: Z-scheme; Surface plasmon resonance (SPR); TiO_2; Photocatalysis; Hydrogen generation

1. Introduction

The rapid consumption of non-renewable fossil fuels and the accompanying environmental pollution are forcing people to find clean and sustainable energy. Due to its high energy storage and environment friendliness, hydrogen is considered to be one of the best potential candidates. Since the electrochemical photolysis of water at TiO_2 electrode was firstly reported by Fujishima and Honda in 1972 [1], numerous efforts have been made to improve the performance of TiO_2 on photocatalytic hydrogen generation, which is mainly restricted by the fast recombination rate of photogenerated electron-hole pairs [2–5]. In recent years, hybrid or multi-component photocatalysts have shown significant advantages in suppressing the recombination of photogenerated electron-hole pairs through an efficient charge transfer process, and thus driving efficient photo-reduction and oxidation reactions at spatially separated sites [4–6]. Therefore, the construction of multi-component photocatalysts is recognized as an effective strategy to enhance the photocatalytic performance of TiO_2.

Cu_2O has been proved to be a good promoter to hybridize with TiO_2 [7–17]. This is because (i) Cu_2O with a narrow band gap of 2.0 eV can extend the absorption to visible-light range with wavelength up to 620 nm; (ii) both the conduction (CB) and valence bands (VB) of Cu_2O lie higher than those of TiO_2, which is favorable for the efficient transfer of excited electrons and holes between each other. Particularly, the excited electrons of Cu_2O transfer to CB of TiO_2 and the excited holes of TiO_2 transfer to the VB of Cu_2O, respectively. This process involves a typical charge transfer mechanism of a semiconductor heterojunction. The Cu_2O/TiO_2 heterojunctions have thus shown greatly enhanced activities as compared to single TiO_2, due to the efficient charge separation between Cu_2O and TiO_2 [7,8,16]. However, it is known that the

* Corresponding authors. State Key Laboratory of Advanced Technology for Materials Synthesis and Processing, Wuhan University of Technology, Wuhan, 430070, PR China. Tel.: +86 27 87871029; fax: +86 27 87879468.
E-mail addresses: swcao@whut.edu.cn (S. Cao), jiaguoyu@yahoo.com (J. Yu).
Peer review under responsibility of The Chinese Ceramic Society.

http://dx.doi.org/10.1016/j.jmat.2015.02.002

electrons in less negative CB and holes in less positive VB show weaker redox ability. Consequently, the resultant shortcoming of the typical semiconductor heterojunction is that the redox ability of transferred electrons and holes are reduced [5,16], which negatively affect the photocatalytic reactions. Thus, developing photocatalytic systems with both fast electron-hole separation and strong redox ability is still a challenge.

A Z-scheme charge transfer mechanism that is different from the typical charge transfer mechanism of a semiconductor heterojunction, has also been proposed and investigated in the past decade. Such a Z-scheme pathway of charge transfer can preserve the oxidative holes in the lower VB and reductive electrons in the higher CB, resulting in not only greatly improved separation efficiency but also strong redox ability of photogenerated electrons and holes. Till now, a number of Z-scheme photocatalytic systems have been reported such as TiO_2/CdS [18,19], ZnO/CdS [20,21], anatase/rutile [22], g−C_3N_4/TiO_2 [23], AgBr/Ag/AgI [24], H_2WO_4•H_2O/Ag/AgCl [25], AgBr/Ag/BiOBr [26], Ag_2CrO_4−GO [27] and $Bi_{20}TiO_{32}$/Ag/AgCl [28], all of which have exhibited much better photocatalytic performance than the single-component photocatalyst. Nevertheless, in a semiconductor heterojunction, the Z-scheme charge transfer process usually faces the competition of the typical charge transfer process [20,29]. In this regard, a conductor or a contact interface with low contact resistance can be applied as an electron mediator to speed up the desirable specific carrier transfer [16,18,19,21,24–26]. For instance, Ag has been used as such mediator in many Z-scheme systems [19,24–27] because it has excellent electron conductivity. In addition, Ag can enhance the absorption of visible light and accelerate the electron transfer by a surface plasmon resonance (SPR)-induced local electric field, for example, anomalous Ag nanoparticles in AgI/Ag/AgBr composite [24], and 5–10 nm sized Ag nanoparticles in H_2WO_4•H_2O/Ag/AgCl composite [25].

In this study, we introduce a dual Z-scheme TiO_2−Ag−Cu_2O photocatalytic system, in which Cu_2O was loaded onto electrospun TiO_2 nanotubes by a facile impregnation-calcination method, and Ag was subsequently deposited onto the photocatalyst through a photodeposition method. Under UV−vis light irradiation, both TiO_2 and Cu_2O can be excited. The photogenerated electrons in the CB of TiO_2 will transfer to Ag due to the formation of Schottky barrier on the metal-semiconductor interface. Meanwhile, the SPR-induced local electric field will drive the electrons of Ag to combine with the holes on the VB of Cu_2O. Finally, electrons on the CB of Cu_2O will react with H^+ to generate H_2. As a result, the TiO_2−Ag−Cu_2O composite shows greatly improved photocatalytic performance for hydrogen generation than TiO_2, TiO_2−Ag, and TiO_2−Cu_2O.

2. Experimental

2.1. Materials

All chemicals were of analytical grade and without further purification. Tetrabutyl titanate ($Ti(OC_4H_9)_4$, TBOT) was purchased from Shanghai Kefeng Industry Co., Ltd. Polyvinylpyrollidone (PVP $Mw = 1.3 \times 10^6$) was purchased from Aladdin Industrial Corporation. Paraffin liquid was purchased from Tianjin Guangcheng Chemical Reagent Co., Ltd. Ethanol (C_2H_5OH) and Copper (II) nitrate trihydrate ($Cu(NO_3)_2.3H_2O$) were purchased from Sinopharm Chemical Regent Co., Ltd. Silver nitrate ($AgNO_3$) was purchased from Tianjin Kemi'ou Chemical Reagent Co., Ltd. Methanol (CH_3OH) was purchased from Tianjin Beichen Founder Reagent Factory. Deionized (DI) water was used in all experiments.

2.2. Preparation of TiO_2 electrospun nanotubes

The TiO_2 nanotubes were prepared by a coaxial electrospinning method modified from that described by Xia et al. [30]. In a typical procedure for electrospinning, the precursor solution consisting of 1 g PVP, 5 mL TBOT, and 10 mL C_2H_5OH was vigorously stirred for 12 h. The solution was then added to a 20 mL syringe connected to the outer capillary of a coaxial two-capillary spinneret. The inner capillary of the two-capillary spinneret was connected to a 2.5 mL syringe filled with paraffin liquid. The diameters of the outer and inner capillaries were 1.6 mm and 0.7 mm, respectively. The feeding rate for PVP solution was set at 1 mL/h. For paraffin liquid, the feeding rate was 0.2 mL/h. Electrospinning was performed at 25 °C for 10 h with an applied potential of 15 kV and a distance of ~10 cm from the tip to the collector. The relative humidity of the electrospinning chamber was kept at ~30%. The as-prepared electrospun nanofibers were kept in air for 2 h to allow the complete hydrolyzation of TBOT precursor. The resultant composite nanofibers consisting of amorphous TiO_2, PVP and paraffin liquid were heated to 500 °C at a rate of 2 °C/min, and kept for 6 h to remove the PVP and paraffin thoroughly. Then the electrospun TiO_2 nanotubes were obtained.

2.3. Preparation of TiO_2−Ag−Cu_2O photocatalyst

The TiO_2−Ag−Cu_2O photocatalyst was prepared from TiO_2 electrospun nanotubes by loading Cu_2O and Ag through impregnation-calcination and photodeposition methods, respectively. Typically, 0.3 g TiO_2 nanotubes were immersed in a $Cu(NO_3)_2$ solution consisting of 4.5 mg $Cu(NO_3)_2.3H_2O$ and 20 mL deionized water. The mixed solution was stirred at 80 °C until the solvent was completely evaporated. The obtained powder was calcined at 350 °C for 4 h to yield Cu_2O/TiO_2 composite. The Cu_2O loading on TiO_2 was estimated to be ca. 0.5% (in mass). Then 0.3 g Cu_2O/TiO_2 powder and 2.4 mg of $AgNO_3$ was added into 16 mL deionized water under magnetic stirring. The Ag loading on TiO_2 was estimated to be ca. 0.5% (in mass). 4 mL methanol was injected into the above suspension, followed by the irradiation of a UV−vis light lamp for 2 h. After that, the suspension was collected and thoroughly rinsed with deionized water and ethanol three times to remove the residual impurity. This sample was denoted as TCA and the original electrospun TiO_2 nanotube was named as T. The electrospun TiO_2 nanotubes

loading with just 1% (in mass) Ag and 1% (in mass) Cu_2O were denoted as TA and TC, respectively.

2.4. Characterization

The X-ray diffraction (XRD) patterns were obtained on a D/Max-RB X-ray diffractometer (Rigaku, Japan) with Cu Kα radiation at a scan rate (2θ) of 0.05(°)/s. The average crystallite sizes were calculated according to the Scherrer equation using the full-width half-maximum data after correcting the instrumental broadening. The morphology observation was performed on an S-4800 field emission scanning electron microscope (FESEM, Hitachi, Japan). Transmission electron microscopy (TEM) and high-resolution transmission electron microscopy (HRTEM) analysis were conducted with a JEM-2100F transmission electron microscope (JEOL, Japan), at an accelerating voltage of 200 kV. The UV–vis diffuse reflectance spectra were obtained on a UV–vis spectrometer (UV2550, Shimadzu, Japan); $BaSO_4$ was used as a reflectance standard. X-ray photoelectron spectroscopy (XPS) measurement was done on a VG ESCALAB210 XPS system with Mg Kα source and all the binding energies were referenced to the C1s peak at 284.8 eV. Raman spectra were recorded on a mirco-Raman spectrometer (Renishaw InVia) in the back-scattering geometry using a 514 nm Ar^+ laser as excitation source. Photoluminescence (PL) emission spectra were taken with a fluorescence spectrophotometer (F-7000, Hitachi, Japan). The production of hydroxyl radicals (•OH) on the surface of the samples TC and TCA were detected by a photoluminescence method using terephthalic acid as a probe molecule [31]. 10 mg photocatalyst was added into 20 mL mixed solution consisting of 5×10^{-4} M terephthalic acid and 2×10^{-3} M NaOH. Under UV–vis light irradiation, the PL emission spectra of generated 2-hydroxyterephthalic acid were measured every 15 min using the excited wavelength of 325 nm. The actual amounts of Ag and Cu in the samples were measured by inductively coupled plasma atomic emission spectrometry (ICP-AES) using an Optima 4300 DV spectrometer (Perkin Elmer), and the results are shown in Table 1.

2.5. Evaluation of photocatalytic activity

The photocatalytic reactions were carried out in a 100 mL Pyrex flask at ambient temperature and atmospheric pressure. The flask was sealed with silicone rubber septums. A 350 W xenon arc lamp was used as a UV–vis light source to trigger the photocatalytic reaction. The distance between the lamp and reactor was set as ~20 cm. In a typical photocatalytic H_2-production experiment, 50 mg as-prepared photocatalyst was firstly suspended in 80 mL mixed aqueous solution containing 16 mL CH_3OH and 64 mL H_2O. Then the reactor was purged with nitrogen gas to ensure an anaerobic condition. After that, the gas-closed flask was irradiated and 0.4 mL gas sample was extracted from the flask at an interval of 1 h. The H_2 amount was analyzed by gas chromatography (GC-14C, Shimadzu, Japan, TCD, with nitrogen as a carrier gas and 5 Å molecular sieve column). The apparent H_2-production quantum efficiency (Q_e) was measured under the above experimental conditions except different light source used. Four UV-LEDs (3 W, 365 nm, Shenzhen LAMPLIC Science Co. Ltd., China) positioned 1 cm away from the reactor in four different directions were used as light sources to trigger the photocatalytic reaction. The focused intensity and areas on the flask for each UV-LED was ca. 70 mW cm^{-2} and 1 cm^2, respectively. The Q_e was calculated according to the following Eq. (1).

$$Q_e = \frac{N_e}{N_p} = \frac{N_m \times 2}{N_p} \times 100\% \quad (1)$$

Where, N_e is number of reacted electrons; N_p is number of incident photons; N_m is number of evolved H_2 molesules.

Table 1
ICP-AES results of samples.

Sample no.	ICP-AES (%, mass fraction)	
	Ag	Cu
T	0	0
TA	0.696	0
TC	0	0.657
TCA	0.342	0.327

3. Results and discussion

3.1. Phase structure and morphology

Fig. 1(a) shows the typical FESEM image of the electrospun TiO_2 nanotubes which are extracted from the sample T. It can be seen that these nanotubes are uniform with large aspect ratios. A clear tubular structure can be observed from the enlarged image shown in the inset. The average diameter and wall thickness of the nanotubes are ~750 nm and ~100 nm, respectively. Fig. 1(b) indicates that the nanotube feature of TiO_2 does not change obviously in the sample TCA. It is noteworthy that there are a number of particles dispersed on the outer surface of the nanotubes, which should be ascribed to Ag and Cu_2O nanoparticles. An in-depth observation was further performed by TEM, as shown in Fig. 1(c and d). The hollow structure of a single nanotube is clearly displayed in Fig. 1(c). The HRTEM image of the selected area in Fig. 1(c) is presented in Fig. 1(d). The lattice fringe of 0.35 nm is consistent with (101) planes of anatase TiO_2, while the lattice fringe of 0.23 nm is assigned to the (111) planes of Ag. And the lattice fringe of 0.21 nm belongs to the (200) planes of Cu_2O. These results confirm the presence of Ag and Cu_2O on the surface of TiO_2 nanotubes. Note that the connections between these components are intimate, and Ag particles mainly exist at the interface of Cu_2O and TiO_2. This is because the photogenerated electrons mainly assemble on the interface of Cu_2O and TiO_2 during the photodeposition process of Ag. Such unique structure is beneficial for the charge transfer among the three components.

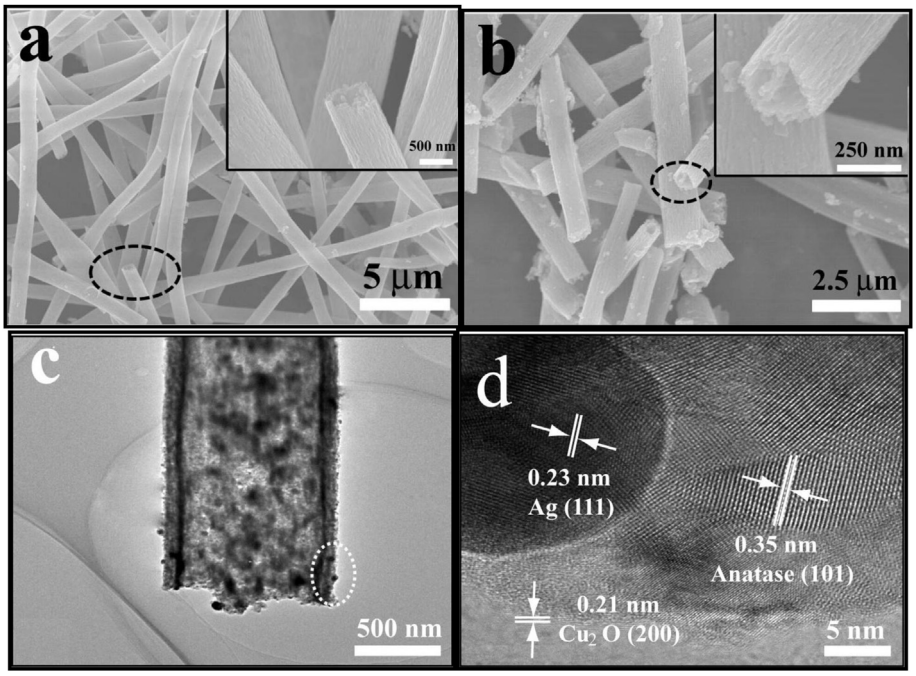

Fig. 1. FESEM images of the sample T (a) and sample TCA (b); TEM (c) and HRTEM (d) images of the sample TCA.

XRD was used to investigate the phase structure and crystallite sizes of the prepared samples. The XRD patterns of the samples T, TA, TC, and TCA are shown in Fig. 2. All of the peaks can be attributed to anatase (JCPDS, No. 21−1272) and rutile phases (JCPDS, No. 21−1276). The co-existence of anatase and rutile can enhance the separation efficient of photo-excited electrons and holes in terms of a mixed-phase heterojunction, which is favorable to improve the photo-catalytic activity [2]. No peaks of copper oxide or silver can be observed, which is due to the low loading amount, small particle size and good dispersion [32]. The average crystallite sizes of anatase and rutile were calculated according to the Scherrer equation using the peaks of anatase (101) and rutile (110), respectively [33,34]. There is no obvious difference of the average crystallite sizes (12−13 nm) among all the samples. The results indicate that the crystal phases and sizes of the electrospun TiO_2 nanotubes are stable during the loading process of copper oxide and silver.

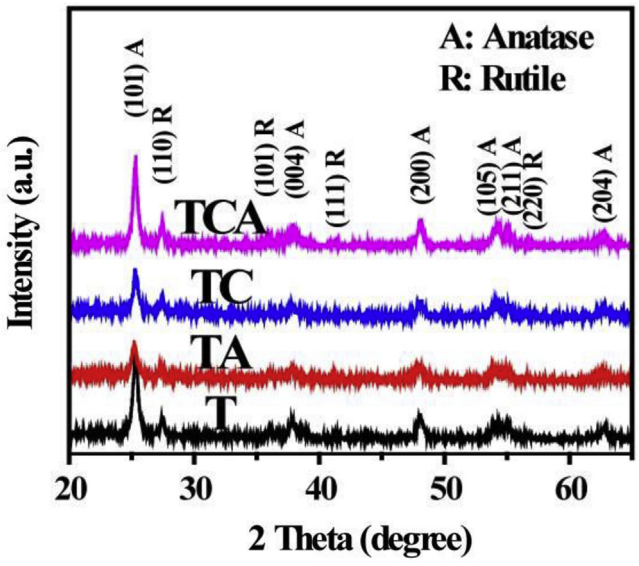

Fig. 2. XRD patterns of the samples T, TA, TC and TCA.

3.2. XPS

XPS was used to identify the chemical status of the elements contained in the samples. The XPS survey spectra (not shown here) confirm the presence of Ag, Cu and Ag/Cu in the samples TA, TC and TCA, respectively. High-resolution XPS spectra of C 1s, O 1s, and Ti 2p for all samples show no obvious changes and thus are also not shown here. In detail, the spectra of C 1s show three peaks at 284.8, 286.0 and 288.9 eV, which are attributed to C−C (adventitious carbon), C−OH (hydroxyl carbon) and O−C═O (carboxyl carbon), respectively [33]. The spectra of O 1s show two peaks at 530.0 and 531.7 eV, which are related to Ti−O−Ti (lattice oxygen) and −OH (hydroxyl oxygen) [35]. The spectra of Ti 2p show two peaks at 458.9 and 464.6 eV, which belong to Ti $2p_{3/2}$ and Ti $2p_{1/2}$. The observed spin-orbit splitting between the Ti $2p_{3/2}$ and Ti $2p_{1/2}$ is 5.7 eV, in good agreement with the value of Ti^{4+} state in TiO_2. Fig. 3(a) shows the high-resolution XPS spectra of Cu 2p. The two main peaks at 932.5 and 952.5 eV are attributed to Cu $2p_{3/2}$ and Cu $2p_{1/2}$, between which there is a weak peak that is the satellite peak of the Cu $2p_{3/2}$ [36,37]. Accordingly, the chemical state of Cu is most probably Cu^+ or Cu^0 in the samples TC and TCA [15,36,38]. It is known that

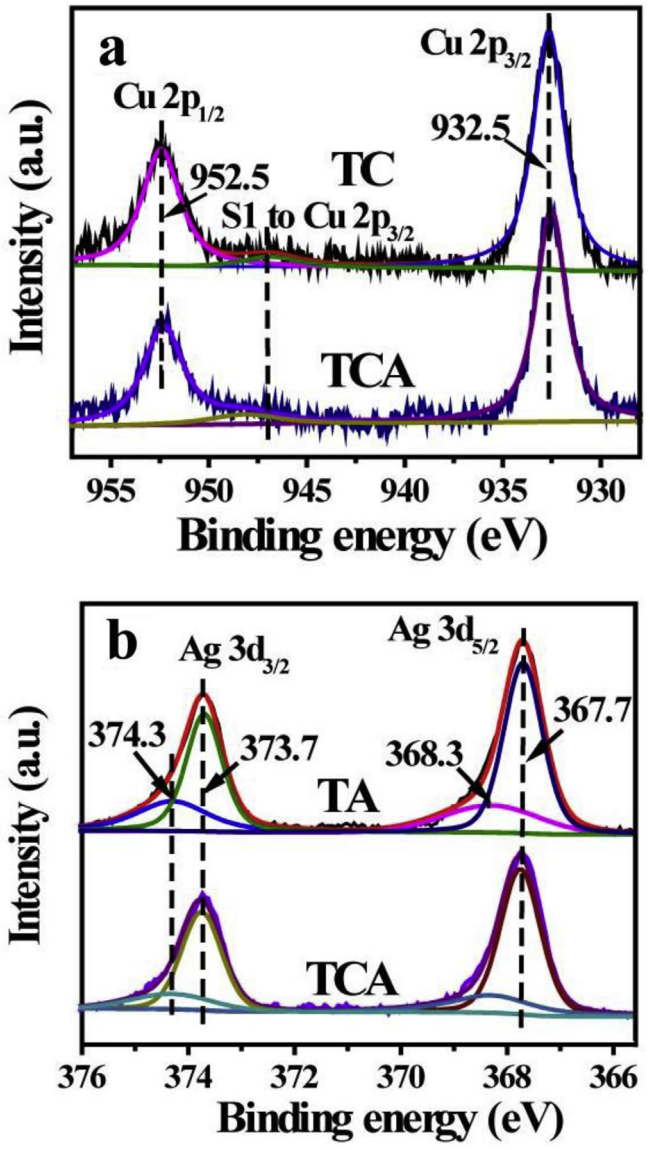

Fig. 3. High-resolution XPS spectra of Cu 2p (a) and Ag 3d (b) for the samples TA, TC and TCA.

Cu^0 is difficult to exist during calcination; and the HRTEM image has also shown clear lattice fringes of Cu_2O. Therefore, the element Cu should mainly exist as Cu^+ in cuprous oxide (Cu_2O) rather than Cu^0. In the high-resolution XPS spectra of Ag 3d (Fig. 3(b)), the two peaks located at 368.3 and 374.3 eV can be assigned to metal Ag species, while the remaining two peaks at 367.7 and 373.7 eV are attributed to Ag^+ which has not been reduced during the photo-reduction process [38].

3.3. UV–vis diffuse reflectance spectra

The comparison of UV–vis diffuse reflectance spectra of the samples is presented in Fig. 4. For all the samples, a significant increase in the absorption region at wavelength shorter than ~410 nm can be assigned to the intrinsic absorption of TiO_2. In particular, the samples TA, TC and TCA exhibit an enhanced light absorption than the sample T in the range of 400–800 nm. This result suggests that loading Cu_2O and Ag can enhance the visible-light absorption which may improve the photocatalytic activity. For the samples TA and TCA, it is noteworthy that there is a broad visible-light absorption band centered at ~500 nm. In order to get an in-depth investigation, the spectra subtracting the contribution of TiO_2 are obtained and shown in Fig. 4(b). The spectrum of TC-T shows an absorption edge at ~620 nm which is in agreement with the intrinsic absorption of Cu_2O, (2.0 eV) [39,40]. Furthermore, the broad absorption bands of the samples TA and TCA in visible-light region are ascribed to the SPR absorption of Ag nanoparticles [19,24–27,41–44]. In addition, the sample TA exhibits a stronger light absorption than sample TCA, which is consistent with the darker color of sample TA with more Ag particles.

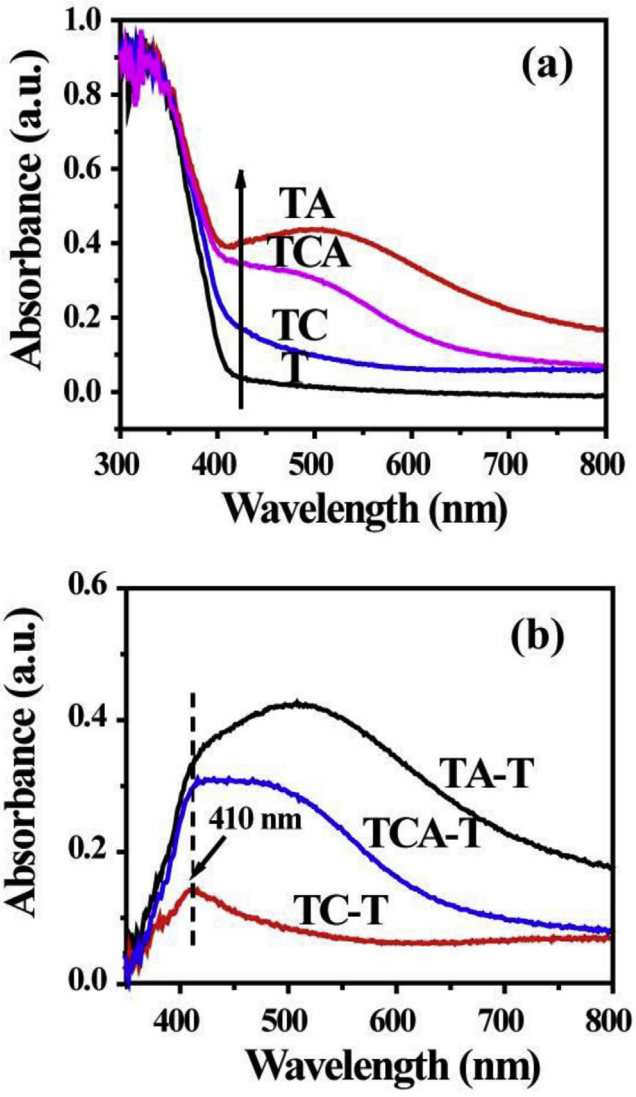

Fig. 4. (a) UV–vis diffuse reflectance spectra of the samples T, TA, TC and TCA. (b) The spectra of TA-T, TC-T, and TCA-T obtained by subtracting the contribution of TiO_2 in the samples TA, TC, TCA.

3.4. Raman analysis

Fig. 5 shows the Raman spectra of the samples T, TA, TC and TCA. The three obvious peaks at around 395 cm^{-1} (B_{1g}), 512 cm^{-1} (A_{1g}) and 637 cm^{-1} ($E_{g(2)}$) can be assigned to anatase [34,45], while the weak signal of rutile is overlapped by that of anatase. It can be found that the Raman signals of samples TA, TC and TCA have been enhanced in comparison with that of sample T, mainly due to the surface-enhanced Raman scattering (SERS). Up to now, there are two possible mechanisms to explain SERS. One is the electromagnetic enhancement caused by the SPR on the metal surface. The other one is the chemical enhancement mechanism including Chemical-Bonding Enhancement, Surface Complexes Resonance Enhancement, and Photo-Induced Charge-Transfer Enhancement (PICT) [46]. Actually, the enhancement of Raman signals by Ag/Cu_2O nanostructure has been reported in a previous literature [47]. Since Fig. 4 has shown that the sample TA exhibits a clear SPR peak of Ag at ~500 nm, it can be inferred that the enhanced Raman signals of sample TA are attributed to the SPR-induced electromagnetic enhancement. While for sample TC, no SPR peak has been observed in the visible-light range. In this case, the PICT process may play an important role on the SERS. As for the sample TCA, the enhancement of TCA should be attributed to the synergetic effect of PICT process of Cu_2O and the SPR-induced electromagnetic effect of Ag.

3.5. Photoluminescence spectra

The PL emission spectra were used to reveal the separation efficiency of photogenerated electron-hole pairs and to understand the lifetime of these photogenerated charge carriers [32,48]. As shown in Fig. 6, all spectra show similar shapes with six main emission peaks attributed to PL signals of TiO_2, appearing at ~398, 410, 451, 468, 483, and 493 nm, respectively. The two peaks at 398 and 410 nm can be assigned to the emission of band gap transition of anatase and rutile. The other four peaks can be ascribed to excitonic PL signals, originating from surface oxygen vacancies and defects of the samples [32]. As compared to sample T, a decrease in emission intensity is observed for sample TC, indicating enhanced separation efficiency of electron-hole pairs in the Cu_2O/TiO_2 composite. The sample TA shows the lowest emission intensity, which reveals that the addition of Ag is effective for separating photogenerated electron-hole pairs, due to the formation of a Schottky barrier at the interface of silver and TiO_2. Therefore, it is not surprising that the sample TCA shows lower emission intensity than sample TC because the photogenerated electrons of TiO_2 can easily transfer to silver.

3.6. Photocatalytic activity

Photocatalytic hydrogen generation on various samples was evaluated under the irradiation of a 350 W xenon arc lamp using methanol as a scavenger. Control experiments indicated that no noticeable hydrogen production was detected in the absence of either irradiation or photocatalyst, suggesting that hydrogen was produced *via* photocatalytic reactions. Fig. 7 shows the comparison of photocatalytic hydrogen generation activity of the as-prepared samples. It can be clearly seen that the loading components has a significant influence on the photocatalytic activity of TiO_2. As compared to the sample T, both samples TA and TC exhibit remarkably enhanced photocatalytic hydrogen production, demonstrating that Ag and Cu_2O can be used as co-catalysts to enhance the photocatalytic hydrogen generation activity [8,49]. Importantly, the highest hydrogen production rate is achieved for the sample TCA, which is owing to the synergetic effect of Ag and Cu_2O on the photocatalytic activity of TiO_2. The corresponding apparent

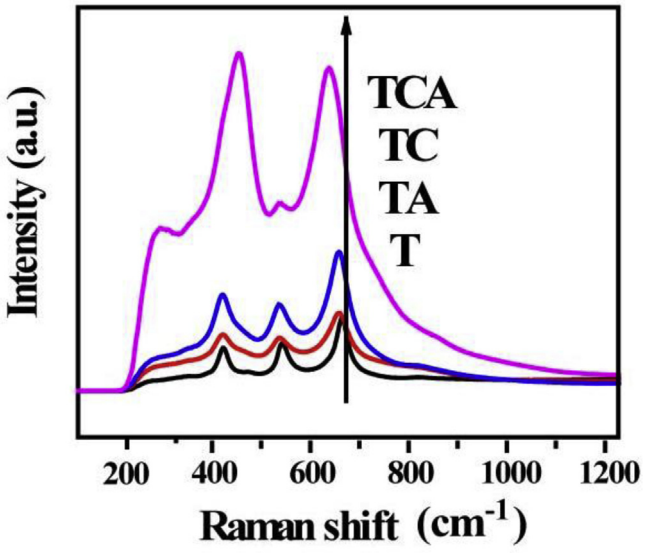

Fig. 5. Raman spectra of the samples T, TA, TC and TCA.

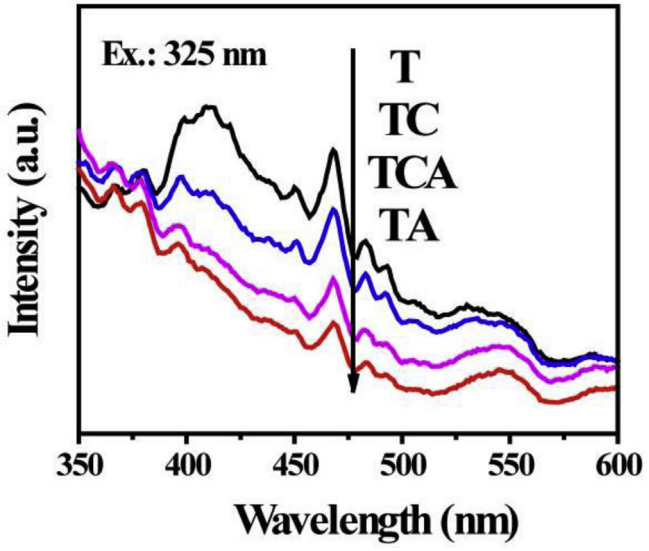

Fig. 6. Comparison of PL spectra of samples T, TA, TC and TCA.

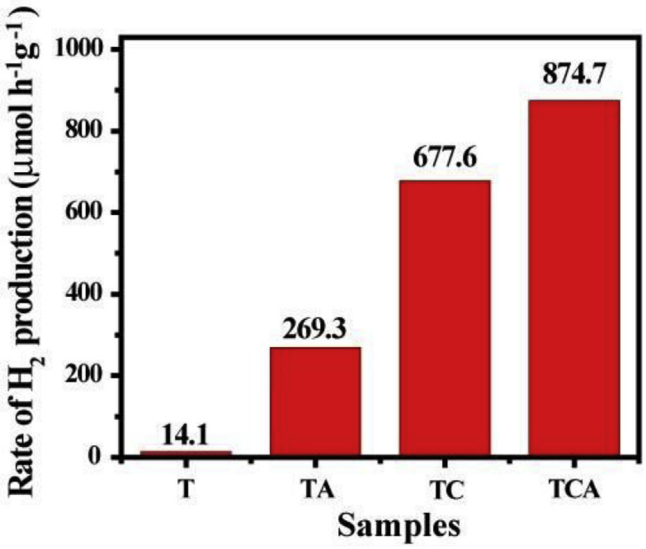

Fig. 7. Photocatalytic hydrogen generation activity of the samples T, TA, TC and TCA.

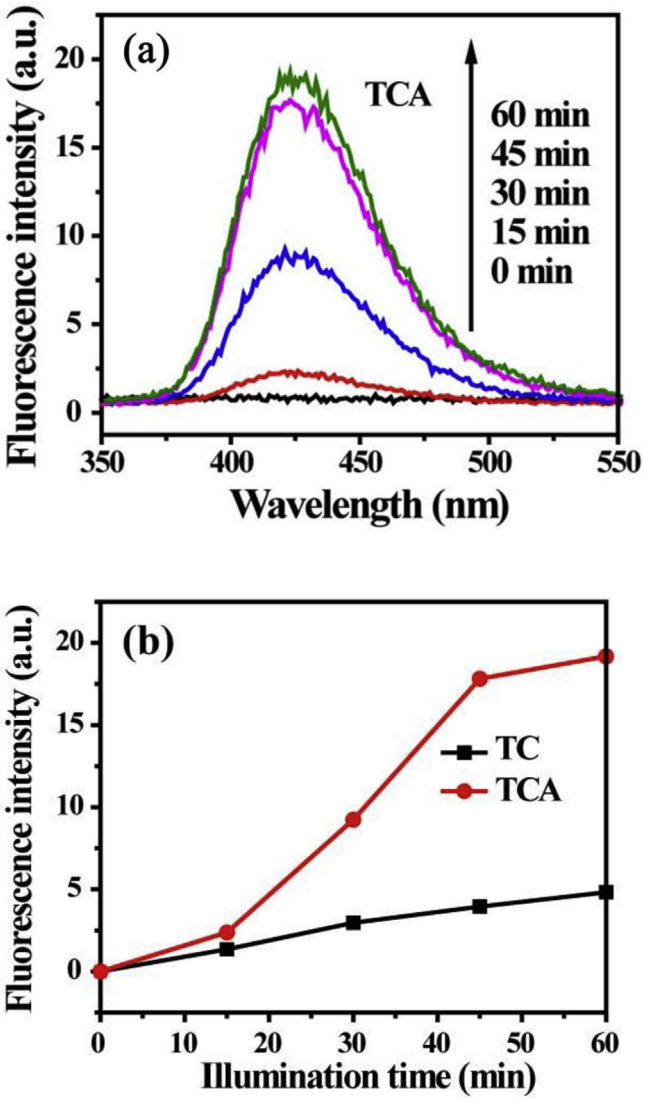

Fig. 8. (a) Changes of PL spectra with UV–vis irradiation time in the presence of TCA sample in a 5×10^{-4} mol/L basic solution of terephthalic acid (excitation at 325 nm); (b) plots of fluorescence intensity at 426 nm *vs.* irradiation time for terephthalic acid on samples TC and TCA.

quantum efficiency of the sample TCA is 2.3% at 365 nm wavelength light irradiation.

It is well known that the separation efficiency of photogenerated electrons-holes plays an extremely important role in photocatalytic hydrogen generation. For example, in the previous report [7], Cu@Cu_2O showed an enhanced effect on the photocatalytic activity of TiO_2, due to the efficient transfer of photo-excited electrons and holes through an Ohmic nanojunction. The best photocatalytic activity of Cu_2O/Cu/TiO_2 exceeded that of pure TiO_2 by about 12 times. In this work, the photocatalytic performance of the sample TCA exceeds that of the sample T by more than 62 times. In order to investigate the charge transfer mechanism, we have measured the formation rates of •OH on the samples TC and TCA in aqueous solutions under the irradiation of xenon lamp by the photoluminescence technique, using terephthalic acid as a probe molecule. Terephthalic acid is a poor fluorescent molecule that could react with •OH to form highly fluorescent 2-hydroxyterephthalic acid. It has been reported that the potential of OH^-/•OH couples is about +2.3 V (*vs.* NHE) [31], lying in between the VB of Cu_2O and that of TiO_2. As such, the holes on the VB of TiO_2 can react with OH^- to generate •OH, while the holes on the VB of Cu_2O is incapable. Fig. 8(a) presents the changes of PL spectra observed during the irradiation on the sample TCA dispersed in terephthalic acid solution. It can be seen that the fluorescence intensity increases significantly with increasing irradiation time. Fig. 8(b) shows the plots of fluorescence intensity at 426 nm versus irradiation time for terephthalic acid in the presence of samples TC and TCA, respectively. The PL in the presence of sample TC shows very low intensity suggesting the low concentration of •OH. Here we assume that the photogenerated charge transfer in the TiO_2/Cu_2O composite follows the typical charge transfer mechanism of a semiconductor heterojunction. When the TiO_2 and Cu_2O are excited by irradiation, the electrons on the CB of Cu_2O will transfer to that of TiO_2; meanwhile, the holes on the VB of TiO_2 will transfer to that of Cu_2O. Consequently, the hole density in the VB of TiO_2 is depleted while that in the VB of Cu_2O is enhanced (Fig. 9(a)). Due to the less positive position of the VB of Cu_2O, the holes on Cu_2O do not have enough energy to oxidize OH^- or H_2O to form •OH. Hence the sample TC has low generation rate of •OH. Contrarily, the fluorescent intensity in the presence of sample TCA is much higher than that in the presence of sample TC. It means that the photogenerated holes of the sample TCA accumulate in the VB of TiO_2, suggesting a different charge transfer mechanism.

On the basis of the above results, a possible photocatalytic mechanism of the sample TCA is proposed and illustrated in Fig. 9(b). Under UV–vis irradiation, both Cu_2O and TiO_2 are

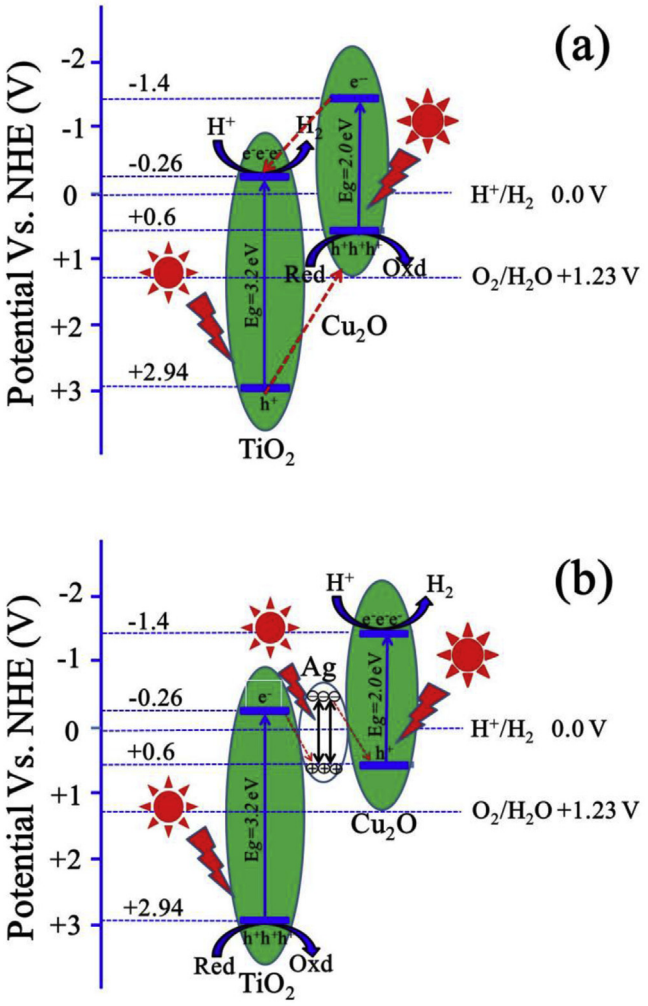

Fig. 9. Schematic illustration for the charge transfer in sample TC (a) and sample TCA (b) under UV–vis light irradiation.

photoexcited to generate electrons and holes. Since equilibrium of the Fermi levels has been established at the interfaces of TiO_2, Ag and CuO before light irradiation, and electrons on the CB of TiO_2 will migrate to Ag after light irradiation. On the other hand, the strong SPR of Ag nanoparticles results in an enhanced local electric field around the interfaces, which can drive the electrons of Ag to inject into the VB of Cu_2O to recombine with holes or into the CB of Cu_2O *via* direct electron transfer or plasmon-induced resonant energy transfer [50]. As a result, the accumulated electrons in the CB of Cu_2O with high potential energy can reduce the H^+ to produce H_2, and the holes left behind the VB can achieve the photo-oxidation process. It is noteworthy that this type of charge transfer pathway retains the photogenerated holes on the more positive VB of TiO_2 and electrons on the more negative CB of Cu_2O, which not only greatly improve the separation of electron-hole pairs, but more importantly can preserve their high redox ability [29,51]. As this charge transfer pathway is analogous to that of the Z-scheme mechanism in a double "Z" shape, we hereby tentatively call it "dual Z-scheme charge transfer".

4. Conclusions

In summary, we construct a multi-component TiO_2–Ag–Cu_2O photocatalytic system based on the electrospun TiO_2 nanotubes by a facile impregnation-calcination route combined with a photodeposition strategy. The TiO_2–Ag–Cu_2O composite exhibits efficient photocatalytic activity for hydrogen generation due to the synergetic effect of Cu_2O and Ag. The introduction of Cu_2O and Ag result in an enhanced visible-light absorption ability and moreover, the SPR-induced local electric field causes a dual Z-scheme charge transfer pathway in the composite, which enables both high separation efficiency and high redox ability of photogenerated electrons and holes. This work demonstrates that the SPR effect of Ag can adjust the transfer of photogenerated electron-hole pairs and provide a new insight into the design of highly efficient photocatalysts for hydrogen generation.

Acknowledgments

This work was supported by the 973 program (2013CB632402), and NSFC (51272199, 51320105001, 51372190, and 21433007). Also, this work was financially supported by the Natural Science Foundation of Hubei Province of China (2014CFB164), Deanship of Scientific Research (DSR) of King Abdulaziz University (90-130-35-HiCi), the Fundamental Research Funds for the Central Universities (WUT: 2014-VII-010, 2014-IV-058, 2014-IV-155), Self-determined and Innovative Research Funds of SKLWUT (2013-ZD-1), and a WUT Start-Up Grant.

References

[1] Fujishima A, Honda K. Electrochemical photolysis of water at a semiconductor electrode. Nature 1972;238:37–8.
[2] Liu J, Yu X, Liu Q, Liu R, Shang X, Zhang S, et al. Surface-phase junctions of branched TiO_2 nanorod arrays for efficient photoelectrochemical water splitting. Appl Catal B: Environ 2014;158–159:296–300.
[3] Linsebigler AL, Lu G, John J, Yates T. Photocatalysis on TiO_2 surfaces: principles, mechanisms, and selected results. Chem Rev 1995;95:735–58.
[4] Chen X, Shen S, Guo L, Mao SS. Semiconductor-based photocatalytic hydrogen generation. Chem Rev 2010;110:6503–70.
[5] Li X, Yu JG, Low JX, Fang YP, Xiao J, Chen XB. Engineering heterogeneous semiconductors for solar water splitting. J Mater Chem A 2015;6:2485–534.
[6] Li X, Wen JQ, Low JX, Fang YP, Yu JG. Design and fabrication of semiconductor photocatalyst for photocatalytic reduction of CO_2 to solar fuel. Sci China Mater 2014;57:70–100.
[7] Li Z, Liu J, Wang D, Gao Y, Shen J. Cu_2O/Cu/TiO_2 nanotube ohmic heterojunction arrays with enhanced photocatalytic hydrogen production activity. Int J Hydrogen Energy 2012;37:6431–7.
[8] Wang Z, Liu Y, Martin DJ, Wang W, Tang J, Huang W. CuO_x-TiO_2 junction: what is the active component for photocatalytic H_2 production. Phys Chem Chem Phys 2013;15:14956–60.
[9] Xiong L, Yang F, Yan L, Yan N, Yang X, Qiu M, et al. Bifunctional photocatalysis of TiO_2/Cu_2O composite under visible light: Ti^{3+} in organic pollutant degradation and water splitting. J Phys Chem Solids 2011;72:1104–9.

[10] Jung M, Scott J, Ng YH, Jiang Y, Amal R. CuO_x dispersion and reducibility on TiO_2 and its impact on photocatalytic hydrogen evolution. Int J Hydrogen Energy 2014;39:12499–506.
[11] Zhang S, Peng F, Zhang H, Liu H, Zhao H. Electrodeposition of polyhedral Cu_2O on TiO_2 nanotube arrays for enhancing visible light photocatalytic performance. Electrochem Commun 2011;13:861–4.
[12] Liu Y, Yang G, Zhang H, Cheng Y, Chen K, Peng Z, et al. Enhanced visible photocatalytic activity of Cu_2O nanocrystal/titanate nanobelt heterojunctions by a self-assembly process. RSC Adv 2014;4:24363–8.
[13] Xi Z, Li C, Zhang L, Xing M, Zhang J. Synergistic effect of Cu_2O/TiO_2 heterostructure nanoparticle and its high H_2 evolution activity. Int J Hydrogen Energy 2014;39:6345–53.
[14] Zhu L, Zhang J, Chen Z, Liu K, Gao H. Effect of Cu_2O morphology on photocatalytic hydrogen generation and chemical stability of TiO_2/Cu_2O composite. J Nanosci Nanotechnol 2013;13:5104–8.
[15] Lalitha K, Sadanandam G, Kumari VD, Subrahmanyam M, Sreedhar B, Hebalkar NY. Highly stabilized and finely dispersed Cu_2O/TiO_2: a promising visible sensitive photocatalyst for continuous production of hydrogen from glycerol:water mixtures. J Phys Chem C 2010;114:22181–9.
[16] Xing J, Chen ZP, Xiao FY, Ma XY, Wen CZ, Li Z, et al. Cu-Cu_2O-TiO_2 nanojunction systems with an unusual electron-hole transportation pathway and enhanced photocatalytic properties. Chem Asian J 2013;8:1265–70.
[17] Liu L, Yang W, Li Q, Gao S, Shang JK. Synthesis of Cu_2O nanospheres decorated with TiO_2 nanoislands, their enhanced photoactivity and stability under visible light illumination, and their post-illumination catalytic memory. ACS Appl Mater Interfaces 2014;6:5629–39.
[18] Tada H, Mitsui T, Kiyonaga T, Akita T, Tanaka K. All-solid-state Z-scheme in CdS-Au-TiO_2 three-component nanojunction system. Nat Mater 2006;5:782–6.
[19] Xie K, Wu Q, Wang Y, Guo W, Wang M, Sun L, et al. Electrochemical construction of Z-scheme type CdS–Ag–TiO_2 nanotube arrays with enhanced photocatalytic activity. Electrochem Commun 2011;13:1469–72.
[20] Wang X, Liu G, Chen ZG, Li F, Wang L, Lu GQ, et al. Enhanced photocatalytic hydrogen evolution by prolonging the lifetime of carriers in ZnO/CdS heterostructures. Chem Commun 2009;23:3452–4.
[21] Wang X, Liu G, Wang L, Chen ZG, Lu GQ, Cheng HM. ZnO–CdS@Cd heterostructure for effective photocatalytic hydrogen generation. Adv Energy Mater 2012;2:42–6.
[22] Xu FY, Xiao W, Cheng B, Yu JG. Direct Z-scheme anatase/rutile bi-phase nanocomposite TiO_2 nanofiber photocatalyst with enhanced photocatalytic H_2-production activity. Int J Hydrogen Energy 2014;39:15394–402.
[23] Yu JG, Wang SH, Low JX, Xiao W. Enhanced photocatalytic performance of direct Z-scheme g-C_3N_4/TiO_2 photocatalyst for decomposition of formaldehyde in air. Phys Chem Chem Phys 2013;15:16883–90.
[24] Lin H, Cao J, Luo B, Xu B, Chen S. Synthesis of novel Z-scheme AgI/Ag/AgBr composite with enhanced visible light photocatalytic activity. Catal Commun 2012;21:91–5.
[25] Wang XF, Li SF, Ma YQ, Yu HG, Yu JG. H_2WO_4•H_2O/Ag/AgCl composite nanoplates: a plasmonic Z-scheme visible-light photocatalyst. J Phys Chem C 2011;115:14648–55.
[26] Ye L, Liu J, Gong C, Tian L, Peng T, Zan L. Two different roles of metallic Ag on Ag/AgX/BiOX (X = Cl, Br) visible light photocatalysts: surface plasmon resonance and Z-scheme bridge. ACS Catal 2012;2:1677–83.
[27] Xu DF, Cheng B, Cao SW, Yu JG. Enhanced photocatalytic activity and stability of Z-scheme Ag2CrO4-GO composite photocatalysts for organic pollutant degradation. Appl Catal B: Environ 2015;164:380–8.
[28] Hou J, Wang Z, Yang C, Zhou W, Jiao S, Zhu H. Hierarchically plasmonic Z-scheme photocatalyst of Ag/AgCl nanocrystals decorated mesoporous single-crystalline metastable Bi20TiO32 nanosheets. J Phys Chem C 2013;117:5132–41.
[29] Zhou P, Yu JG, Jaroniec M. All-solid-state Z-scheme photocatalytic systems. Adv Mater 2014;26:4920–35.
[30] Li D, Xia YN. Direct fabrication of composite and ceramic hollow nanofibers by electrospinning. Nano Lett 2004;4:933–8.
[31] Xiang QJ, Yu JG, Wong PK. Quantitative characterization of hydroxyl radicals produced by various photocatalysts. J Colloid Interf Sci 2011;357:163–7.
[32] Yu JG, Hai Y, Jaroniec M. Photocatalytic hydrogen production over CuO-modified titania. J Colloid Interf Sci 2011;357:223–8.
[33] Fu JW, Cao SW, Yu JG, Low JX, Lei YP. Enhanced photocatalytic CO_2-reduction activity of electrospun mesoporous TiO_2 nanofibers by solvothermal treatment. Dalton Trans 2014;43:9158–65.
[34] Xue X, Ji W, Mao Z, Mao H, Wang Y, Wang X, et al. Lombardi, Raman investigation of nanosized TiO_2: effect of crystallite size and quantum confinement. J Phys Chem C 2012;116:8792–7.
[35] Dai GP, Yu JG, Liu G. Synthesis and enhanced visible-light photoelectrocatalytic activity of p-n junction BiOI/TiO_2 nanotube arrays. J Phys Chem C 2011;115:7339–46.
[36] Pauly N, Tougaard S, Yubero F. Determination of the Cu 2p primary excitation spectra for Cu, Cu_2O and CuO. Surf Sci 2014;620:17–22.
[37] Huang L, Peng F, Ohuchi FS. In situ XPS study of band structures at Cu_2O/TiO_2 heterojunctions interface. Surf Sci 2009;603:2825–34.
[38] Moulder JF, Stickle WF, Sobol PE, Bomben KD. Handbook of X-ray photoelectron spectroscope. Perkin Elmer Eden Prairie Minnesota; 1992.
[39] Cheng WY, Yu TH, Chao KJ, Lu SY. Cu_2O-decorated mesoporous TiO_2 beads as a highly efficient photocatalyst for hydrogen production. Chem Cat Chem 2014;6:293–300.
[40] Huang L, Peng F, Wang H, Yu H, Li Z. Preparation and characterization of Cu_2O/TiO_2 nano–nano heterostructure photocatalysts. Catal Commun 2009;10:1839–43.
[41] Low JX, Yu JG, Li Q, Cheng B. Enhanced visible-light photocatalytic activity of plasmonic Ag and graphene co-modified Bi_2WO_6 nanosheets. Phys Chem Chem Phys 2014;16:1111–20.
[42] Xiang QJ, Yu JG, Cheng B, Ong HC. Microwave-hydrothermal preparation and visible-light photoactivity of plasmonic photocatalyst Ag-TiO_2 nanocomposite hollow spheres. Chem Asian J 2010;5:1466–74.
[43] Hirakawa T, Kamat PV. Photoinduced electron storage and surface plasmon modulation in Ag@TiO_2 clusters. Langmuir 2004;20:5645–7.
[44] Hirakawa T, Kamat PV. Charge separation and catalytic activity of Ag@TiO_2 core-Shell composite clusters under UV-Irradiation. J Am Chem Soc 2005;127:3829–34.
[45] Ohsaka T, Izumi F, Fujiki Y. Raman spectrum of anatase, TiO_2. J Raman Spectrosc 1978;7:321–4.
[46] Wang X, Shi W, She G, Mu L. surface-enhanced Raman scattering (SERS) on transition metal and semiconductor nanostructures. Phys Chem Chem Phys 2012;14:5891–901.
[47] Ji R, Sun W, Chu Y. One-step hydrothermal synthesis of Ag/Cu_2O heterogeneous nanostructures over Cu foil and their SERS applications. RSC Adv 2014;4:6055–9.
[48] Yu JG, Ran JR. Facile preparation and enhanced photocatalytic H_2-production activity of $Cu(OH)_2$ cluster modified TiO_2. Energy Environ-Sci 2011;4:1364–71.
[49] Wu F, Hu X, Fan J, Liu E, Sun T, Kang L, et al. Photocatalytic activity of Ag/TiO_2 nanotube arrays enhanced by surface plasmon resonance and application in hydrogen evolution by water splitting. Plasmonics 2012;8:501–8.
[50] Li J, Cushing SK, Bright J, Meng F, Senty TR, Zheng P, et al. Ag@Cu_2O core-shell nanoparticles as visible-Light plasmonic photocatalysts. ACS Catal 2013;3:47–51.
[51] Chen S, Hu Y, Ji L, Jiang X, Fu X. Preparation and characterization of direct Z-scheme photocatalyst $Bi_2O_3/NaNbO_3$ and its reaction mechanism. Appl Surf Sci 2014;292:357–66.

Jiaguo Yu received his BS and MS in chemistry from Central China Normal University and Xi'an Jiaotong University, respectively, and his PhD in Materials Science in 2000 from Wuhan University of Technology. In 2000, he became a Professor at Wuhan University of Technology. He was a post-doctoral fellow at the Chinese University of Hong Kong from 2001 to 2004, a visiting scientist from 2005 to 2006 at University of Bristol, a visiting scholar from 2007 to 2008 at University of Texas at Austin. His current research interests include semiconductor photocatalysis, photocatalytic solar fuel production and so on. See more details on: http://www.researcherid.com/rid/G-4317-2010.

Junwei Fu obtained his B.S degree in materials science and engineering from Hubei University of Technology in 2012. From 2012 to present, he studies in Prof. Yu's group as a master candidate in Wuhan University of Technology. His current research focuses on the synthesis and properties of photocatalytic materials.